

Ellipsometry-based combination of isothermal sorption-desorption measurement and temperature programmed desorption technique: A probe for interaction of thin polymer films with solvent vapor

Mikhail Yu. Efremov, and Paul F. Nealey

Citation: [Review of Scientific Instruments](#) **89**, 055114 (2018); doi: 10.1063/1.5021269

View online: <https://doi.org/10.1063/1.5021269>

View Table of Contents: <http://aip.scitation.org/toc/rsi/89/5>

Published by the [American Institute of Physics](#)

PHYSICS TODAY

WHITEPAPERS

MANAGER'S GUIDE

Accelerate R&D with
Multiphysics Simulation

READ NOW

PRESENTED BY

 **COMSOL**

Ellipsometry-based combination of isothermal sorption-desorption measurement and temperature programmed desorption technique: A probe for interaction of thin polymer films with solvent vapor

Mikhail Yu. Efremov^{1,a)} and Paul F. Nealey²

¹College of Engineering, University of Wisconsin–Madison, Madison, Wisconsin 53706, USA

²Institute for Molecular Engineering, University of Chicago, 5640 South Ellis Ave., Chicago, Illinois 60637, USA

(Received 2 January 2018; accepted 30 April 2018; published online 22 May 2018)

An environmental chamber equipped with an *in situ* spectroscopic ellipsometer, programmatic vapor pressure control, and variable temperature substrate holder has been designed for studying polymer coating behavior during an exposure to a solvent vapor and also for probing the residual solvent in the film afterwards. Both sorption-desorption cycle at a constant temperature and temperature programmed desorption (TPD) of the residual solvent manifest themselves as a change of the film thickness. Monitoring of ellipsometric angles of the coating allows us to determine the thickness as a function of the vapor pressure or sample temperature. The solvent vapor pressure is precisely regulated by a computer-controlled pneumatics. TPD spectra are recorded during heating of the film in an oil-free vacuum. The vapor pressure control system is described in detail. The system has been tested on 6–170 nm thick polystyrene, poly(methyl methacrylate), and poly(2-vinyl pyridine) films deposited on silicon substrates. Liquid toluene, water, ethanol, isopropanol, cyclohexane, 1,2-dichloroethane, and chlorobenzene were used to create a vapor atmosphere. Typical sorption-desorption and TPD curves are shown. The instrument achieves sub-monolayer sensitivity for adsorption studies on flat surfaces. Polymer-solvent vapor systems with strong interaction demonstrate characteristic absorption-desorption hysteresis spanning from vacuum to the glass transition pressure. Features on the TPD curves can be classified as either glass transition related film contraction or low temperature broad contraction peak. Typical absorption-desorption and TPD dependencies recorded for the 6 nm thick polystyrene film demonstrate the possibility to apply the presented technique for probing size effects in extremely thin coatings. *Published by AIP Publishing.* <https://doi.org/10.1063/1.5021269>

I. INTRODUCTION

The traditional field of polymer-solvent interaction is back into research focus due to advancements in nanolithography techniques. Phase separation in thin (tens of nanometers thick) films of certain block-copolymers (BCPs) opens a new route to achieve extremely fine lithographic patterns.^{1–5} Annealing of BCP films on a substrate in a solvent vapor is a key procedure to achieve a phase separation under mild conditions.^{1,3,6} A majority of publications in this field are focused on the quality of the pattern as a result of the phase separation. The information about the underlying physics of polymer film-solvent vapor interaction is very scarce despite the potential application for process optimization. Better understanding of polymer film behavior under a tightly regulated vapor atmosphere is an important purpose of the instrument discussed in this paper.

Physical changes in thin supported polymer films exposed to a solvent vapor may be substantially different from the extensively studied bulk polymer samples. Swelling and drying of macroscopic pieces of polymers are often limited by the diffusion of the solvent molecules coupled with the mechanical deformation of the material.⁷ By contrast, the factors of free surface, interface, and confinement became significant for thin coatings.^{8–11} Low mass and high surface-to-volume

ratio in the films present many experimental challenges. The samples can be easily contaminated and oxidized.^{12,13} A limited number of analytical techniques can monitor changes in nanometers-thick films. Film thickness and mass density are natural indicators of swelling and desorption processes in coatings. *In situ* ellipsometry is one of the most informative non-destructive methods to access these parameters in very thin films.^{14,15} Applications of this technique to study swelling in polymer films are reported in the literature—see review.¹⁶ Using *in situ* ellipsometry is also well documented for closely related fields of surface adsorption^{17,18} and thin film porosimetry.^{19,20} However, the experiments involving the precise and programmatic control of the vapor pressure in contact with the sample are scarce.¹⁶ An *in situ* ellipsometer complemented with a computer-controlled vapor pressure regulation system described here offers adequate repeatability of experiments and allows researchers to create sophisticated pressure programs.

An important and unique feature of the presented instrument is the ability to perform temperature programmed desorption (TPD) studies of the residual solvent in the vapor-treated polymer. This is accomplished by a programmatic temperature control of a sample holder in a high ($>10^{-6}$ Torr) oil-free vacuum. Sequential application of vapor exposure and TPD to the same sample without removing it from the chamber can be used for direct comparison between the solvent vapor and

^{a)}E-mail: efremov@wisc.edu

thermal annealing methods. Desorption temperature and amount of solvent captured during the vapor treatment can characterize the effectiveness of solvent annealing. Overall, this combined technique presents a promising way of systematic investigation of solvent vapor-polymer coating interaction.

A similar combination of gas and thermal treatment techniques based on a mechanical dilatometer is reported.^{21,22} The design is successfully used to study structural recovery responses of macroscopic polymer glass samples to gas pressure jumps and temperature jumps. It is shown that the responses are different for these stimuli and do not fit existing models.^{21–23}

Search for the unique effects in extremely thin polymer films can be another interesting application of the presented instrument. Solvent molecules can be viewed as fine penetration probes testing nanometer-sized polymer layers for properties different from the bulk state. This approach is conceptually close to monitoring gold nanospheres captured by the surface of glass-forming polymers for analysis of polymer dynamics in confinement.²⁴

II. EXPERIMENTAL SECTION

A. Vacuum setup and *in situ* ellipsometry

The instrument is based on the existing *in situ* ellipsometry setup combined with the new custom-made solvent vapor pressure control system. The initial station is described in detail elsewhere.¹⁵ In brief, the setup consists of a vacuum chamber with a sample holder inside and 2 flat window assemblies placed at fixed 70° angles of incidence. The holder has 2 cartridge heaters, a connection to an external chiller, and can accommodate truncated 2" wafers. The probing light of the spectroscopic phase-modulated ellipsometer (based on the optical parts of the commercial Verity Instruments ST-10 instrument) enters the chamber through one of the windows, reflects from the sample surface, and exits from the second window to the analyzer and detector. A combination of a two-stage scroll pump, turbo-pump, and liquid nitrogen trap produces an oil-free vacuum better than 10⁻⁶ Torr. Extensive usage of the vacuum system for holding and pumping substantial volumes of solvent vapor limits the vacuum achievable in the chamber. A proportional integral derivative (PID) temperature controller regulates the chiller bath temperature and the current through the heaters to achieve a desired temperature run profile.

B. Solvent vapor pressure control system

Direct evaporation of a liquid solvent into vacuum and two-stage pressure regulation are employed. The schematic of the system is given in Fig. 1. Oil-free vacuum pumps P1–P3 are used for the system evacuation. P1 is a roughing scroll pump Leybold Scrollvac SC 15D, P2 is a hybrid turbomolecular-drug pump Leybold TW70H, and P3 is a liquid nitrogen trap. A computer controls the setup via electro-pneumatic 2-position (on-off) valves V1, V4–V9, V11, V12 and electromagnetic proportioning valve V3. Valves V1 and V5–V7 are Ø1.5" port angle vacuum valves; V8 is an Ø0.75" port angle vacuum

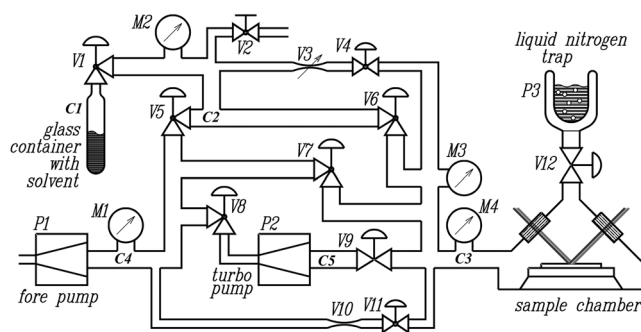


FIG. 1. Sketch of the solvent vapor pressure control system.

valve; V9 and V12 are Ø1.5" port gate vacuum valves; V4, V11, and manual valve V2 are Swagelok SS-BNS4 bellows-sealed valves with an Ø4 mm orifice. V3 is an Omega PSV-5 valve with an Ø3.18 mm orifice and a FSV-10 driver module. V10 is a manual metering valve with an Ø4.2 mm orifice. The computer measures vapor pressure by transducers M2 (MKS Baratron type 626B, 0–1000 Torr range) and M3 (MKS Baratron type 122A, 0–100 Torr range). Analog-to-digital signal conversion for M2 and M3 is performed by using a MKS PDR2000 dual capacitance manometer.

Vacuum in the system is monitored by using gauges M1 (Granville-Phillips Convectron) and M4 (Granville-Phillips Micro-ion gauge). A Pyrex glass tube sealed at one end is used as a liquid solvent container. The tube has a glass to stainless steel 304 ConFlat 1.33" flange adapter (MDC Vacuum) for connection to the vacuum valve. Most connections in the system are made using commercial 2.75" ConFlat-flanged components sealed by using copper gaskets.

The system volume consists of 5 parts with distinct functions. C1 is a glass container with a solvent to be evaporated. Auxiliary volume C2 is confined between the valves V1, V2, and V4–V6. It is primarily used for initial vapor accumulation and the rough pressure regulation. Sample volume C3 is confined between the valves V4, V6, V7, V9, V11, and V12; it includes the sample chamber volume. The pressure in C3 is the target parameter of the regulation system. Rough vacuum compartment C4 is situated between the pump P1 and valves V5, V7, V8, and V11. The space between valves V8 and V9 including the pump P2 defines the turbo pump compartment C5.

A simple vapor pressure program consists of 4 segments: ramp-up, isobaric, ramp-down, and vacuum. The ramp-up segment increases the pressure P in the sample chamber from 0 to P_{ISO} with a constant rate v_{UP} . The isobaric segment keeps $P = P_{ISO}$ for an arbitrary time t_{ISO} . The ramp-down segment reduces P from P_{ISO} to 0 with a constant rate v_{DOWN} . The vacuum segment has 2 options: pumping the sample by the roughing pump only or using all 3 pumps to maintain high vacuum in the sample compartment. The latter option is necessary to prevent polymer sample oxidation at elevated temperatures.

There are 2 loops of the pressure regulation. A rough pressure regulation in the C2 compartment is active during ramp-up and isobaric segments. The regulation algorithm employs an on-off control of the V1 valve. V1 is open if

$P_{C2} < P_{ISO} + \delta P_{LoLim}$ and closed if $P_{C2} > P_{ISO} + \delta P_{HiLim}$. Here, P_{C2} is the solvent vapor pressure in the volume C2; δP_{LoLim} and δP_{HiLim} are constants; the typical values are 5 and 10 Torr, respectively. The typical values here and below are given for toluene vapor and standard program parameters $v_{UP} = 4$ Torr/min, $P_{ISO} = 22$ Torr, $t_{ISO} = 10$ min, and $v_{DOWN} = -4$ Torr/min. A fine pressure regulation in the sample compartment C3 utilizes a proportional-integral (PI) control of the valves V3, V4, and V11. In a control cycle, the program calculates a current P set point P_{SP} determined by the rate setting v , compares it to the actual P measured by M3, and generates the signal to the valves. The vapor flows from C2 to C3 through V3 and V4 during the ramp-up and isobaric segments. C2 is pumped down during the ramp-down segment; the flow direction is reversed. The vapor flow through V3 is regulated continuously. However, the flow through a proportioning valve (V3) cannot be made arbitrarily small. In case when the required flow is less than the V3 low limit, the software uses pulse-width modulation (PWM) of the valve V4. Tighter pressure control during the isobaric segment is achieved by adding a way for the vapor excess to escape from the C3 through valves V10 and V11. Valve V11 is PWM controlled while V10 opening is set manually before the run. The parasitic volumes between V3 and V4 and between V10 and V11 should be minimized for more precise V4 and V11 PWM regulation, respectively.

The initial condition for the ramp-up segment is as follows: all parts of the system are under vacuum and all valves are closed except the turbo backing valve V8. Immediately before the ramp-up segment, V1 opens and fills the volume C2 with the solvent vapor. During the ramp-up segment, valves V3 and V4 are regulated to reach v_{UP} pressure increase rate. Abrupt switching from the ramp-up regime to the following isobaric segment can result in a pressure overshoot condition at a high enough rate v_{UP} . To minimize the overshoot, the program uses low rate v_{UP2} for P_{SP} in the $[(P_{ISO} - \delta P_{UP2}), P_{ISO}]$ interval, where δP_{UP2} is a small constant. Typical values $v_{UP2} = 0.5$ Torr/min and $\delta P_{UP2} = 0.25$ Torr. During the isobaric segment, valves V3, V4, and V11 are closed if P is in the $(P_{ISO} \pm \delta P_{ISODev})$ range, where allowable deviation magnitude δP_{ISODev} is a small constant (typically, 0.03 Torr). If $P < (P_{ISO} - \delta P_{ISODev})$, the algorithm turns on vapor flow into C3 through V3 and V4 with the target rate v_{ISO} (typically, 0.5 Torr/min). Similarly, the condition $P > (P_{ISO} + \delta P_{ISODev})$ forces pumping C3 down through V10 and V11 with the target rate $-v_{ISO}$. The ramp-down segment starts with opening V5 and fast pumping down the C2. The turbo backing V8 should be closed for the moment of high vapor pressure in the fore line C4. Valves V3 and V4 are regulated to reach v_{DOWN} pressure decrease rate. At some point P becomes so close to 0 that even fully open valve V3 cannot maintain programmed v_{DOWN} . Further pumping continues through the roughing valve V7. Program parameter $P_{DOWNLow}$ defines the pressure range $[P_{DOWNLow}, 0]$ when V7 is open during the ramp-down segment. Valves V5, V7, and V8 stay open for the next vacuum segment if roughing the sample compartment is needed. The ultimate vacuum can be achieved by opening V9 and V12, while V5 and V8 stay open. This is a standard configuration for all TPD experiments.

Calibration of the pressure control system is significantly simplified by the following approximation. It assumes that the vapor mass flow through orifices V3 and V10 obeys the equation for the choked (or critical) flow regime: $u = K_1 * P_{UpStr}$, where u is the mass flow rate, P_{UpStr} is the upstream pressure, and K_1 is a constant.^{25,26} As a rule of thumb,²⁶ the choked flow occurs at $P_{UpStr}/P_{DnStr} > 2$, which holds at least for the beginning of the ramp-up segment and for the whole ramp-down segment. There is no abrupt flow rate change at the crossover of the choked and non-choked regimes.^{25,26} A PI algorithm described below demonstrates good adaptation to the gradual regime change during the pressure run. As a result, the choked flow approximation in combination with the PI algorithm can be successfully used for all practical combinations of P_{UpStr} and P_{DnStr} in a pressure run.

The volume of C3 compartment is constant and vapor pressure is proportional to its mass density. Then, the equation for the choked flow can be rewritten as $v/P_{UpStr} = K_2$, where v is the C3 pressure rate and K_2 is a constant. To calibrate the V3 valve, C2 is filled with toluene vapor, C3 is pumped by using P1 via V7, valve V4 is open, a fixed control signal S_{V3} in the 0–1 V DC range is applied to the V3 driver module causing vapor flow from C2 to C3 via V3, and all other valves are closed. Measured 10–15 datapoints of $K_{2,V3} = (V_{C2}/V_{C3}) * (dP_{C2}/dt)/P_{C2}$ as a function of S_{V3} create a calibration table for V3, $K_{2,V3}(S_{V3})$. Here V_{C2}/V_{C3} is the C2 and C3 volume ratio and t is time. V_{C2}/V_{C3} is determined in a separate experiment from a pressure drop associated with expansion of gas from the C2 to the empty C3 volume. Similarly, to calibrate the V10 valve, the C3 is filled with toluene vapor, valve V11 is open, V10 dial is set to a certain position within the useful range of vapor flow (close to the V3 flow range), and all other valves are closed. Several measured datapoints of $K_{2,V10} = (dP_{C3}/dt)/P_{C3}$ as a function of V10 dial position S_{V10} make up the calibration table for V10, $K_{2,V10}(S_{V10})$. During a pressure run, the control algorithm monitors the error signal $(P_{SP} - P)$ and calculates the control output as

$$K_{OUT} = k \left[v + K_P(P_{SP} - P) + K_I \int_{t_0}^t (P_{SP} - P) dt + K_0 \right] / P_{UpStr}, \quad (1)$$

where K_P and K_I are proportional and integral control coefficients, respectively, and t_0 is the segment start time. Constants K_P and K_I are 10 min^{-1} and 100 min^{-2} , respectively. They are found for the standard toluene vapor pressure program by the Ziegler-Nichols tuning method.^{27,28} K_0 is a constant for each segment, added to minimize the pressure overshoot; for isobaric segment K_0 is equal to the final integral term from the previous ramp-up segment. Optimal K_0 for the ramp-up and ramp-down segments are found to be -2 Torr/min and -3.8 Torr/min, respectively. The sign coefficient $k = +1$ if the regulated flow increases P and $k = -1$ otherwise. For the vapor flow through the valve V3, interpolation of the V3 calibration table gives S_{V3} control signal. If $K_{OUT} < K_{2,V3}(0)$ (fully closed V3), the program switches to the V4 PWM control with the $(1 - K_{OUT}/K_{2,V3}(0))$ duty cycle. Similarly, for the vapor flow through valves V10 and V11, the duty cycle of the V11 PWM control signal is equal to $(1 - K_{OUT}/K_{2,V10})$, where $K_{2,V10}$

is defined by the current V10 dial setting. The PWM period (1.6 s) is chosen to be equal to the reciprocal sampling rate of the PDR2000 manometer.

C. Tests of the solvent vapor pressure control system

The system was tested for toluene, 1,2-dichloroethane, cyclohexane, isopropanol, water, ethanol, and chlorobenzene. Maximal tested ramp rates are ± 4 Torr/min, minimal rates are ± 0.3 to ± 0.03 Torr/min depending on the solvent. P_{ISO} for each solvent was chosen to be equal to the saturation pressure P_{SAT} at 17–20 °C. All other run parameters (except v_{UP} , v_{DOWN} , and P_{ISO}) were typical—see Sec. II B. All system parameters, including P and P_{SP} , were recorded during the runs at 1 s intervals. Performance of the control system was characterized by analysis of the error signal $P_{SP} - P$.

The test run for toluene at maximal ramp rates is shown in Fig. 2. Plots (b)–(e) present the details of the transitions between control regimes. Both the ramp-up and ramp-down segments [Figs. 2(b) and 2(d), respectively] start with a small P overshoot. The overshoot at the beginning of the isobaric segment is damped by using $v_{UP2} = 0.5$ Torr/min rate for the last part [21.75 Torr, 22 Torr] of the ramp-up segment [Fig. 2(c)]. Increased P deviation at the end of the ramp-down segment [Fig. 2(e)] is due to the flow limitation when the difference between the up-stream and down-stream pressures is vanishing.

Characteristics of the error signal $P_{SP} - P$ for 19 test runs using different solvents can be found in the [supplementary material](#), Tables 1 and 2. The first runs testing maximal or minimal ramp rates for a given solvent are selected for the

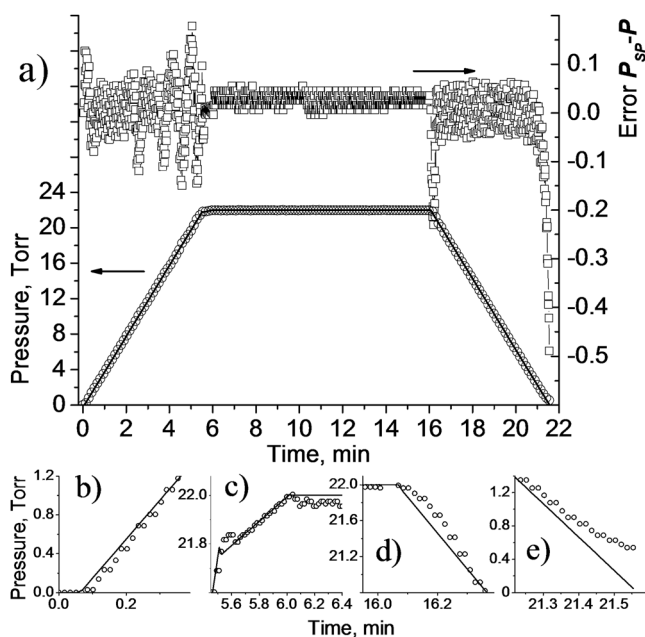


FIG. 2. Toluene vapor pressure test run. Entire run (a): pressure set (solid line), actual pressure (circles), and control errors (squares). Detailed views: the ramp-up segment start (b), switch from the ramp-up segment to the isobaric one (c), the ramp-down segment start (d), and the ramp-down segment end (e). Run parameters: $v_{UP} = 4$ Torr/min, $P_{ISO} = 22$ Torr, $t_{ISO} = 10$ min, and $v_{DOWN} = -4$ Torr/min.

tables. The data demonstrate that the deviation at the end of the ramp-down segment significantly decreases for low ramp rates. The overshoots at the beginning of ramp-up and ramp-down segments are also typically smaller for low rates. The absolute value of the error signal for the pressure ramps does not exceed 0.6 Torr and much smaller for the isobaric segment. The standard deviation for the error signal does not exceed 0.1 Torr for the ramp-up segments in 16 runs and for the ramp-down segments in all cases. The standard deviation for the isobaric segments does not exceed 0.02 Torr. No pressure runaway events were observed. Overall, the performance of the pressure control system is sufficient for the exploratory polymer film–solvent vapor interaction experiments. The system demonstrated adequate pressure control even if the typical regulation settings were applied to different solvents and ramp rates.

D. Limitations of the design

1. Allowable solvents

The materials in contact with the solvents are the following: 300 series stainless steel, 6061 aluminum alloy, and oxygen-free high-conductivity (OFHC) copper (main construction materials); silicate glass (solvent container, wire insulation, and gauges); fused silica (optical windows); ceramics (cartridge heaters and vacuum feedthroughs); Y_2O_3 , Al_2O_3 , Ir, Au, W, Ta, Ni and nickel alloys, and polyimide (pressure gauges); and viton (o-ring seals). The presence of FKM elastomer (ASTM classification of viton²⁹) greatly reduces the variety of solvents suitable for the design. Viton is compatible with water, alcohols, hydrocarbons, and chlorinated hydrocarbons.³⁰ Perfluoroelastomers or FFKM (ASTM classification²⁹) are a good choice for virtually all common solvents including ketones, ethers, esters, amides, and nitriles.³⁰ FFKM materials are available under trade names Kalrez,³¹ Chemraz,³² Parofluor,³³ and others. Currently, solvent resistant analogs for all components used in the system (o-rings, valves, KF flange seals, and scroll vacuum pump) are available commercially.

2. Vapor mixtures

Evaporation of azeotropes can be used in the current design to generate vapor mixtures with specific compositions.

3. Vapor pressure range limitations

The saturation pressure P_{SAT} over the coldest part of the system limits the pressure achievable in the sample compartment. P_{SAT} at room temperature (RT) limits the pressure range for the samples kept at the elevated temperatures. Stabilizing the sample temperature T below RT requires a cooling agent with temperature $T_C < T$. A significant heat loss through the vapor requires T_C to be substantially lower than T especially when a tight temperature control of the sample is needed. Then, P_{SAT} at T_C limits the vapor pressure range.

III. RESULTS AND DISCUSSION

The performance of the combination of the vapor pressure control system, *in situ* ellipsometry in the controlled

atmosphere, and variable temperature sample holder is demonstrated by two types of experiments: (1) sorption and desorption of a vapor on a supported polymer film at a constant temperature and (2) temperature-programmed desorption (TPD). Atactic poly(methyl methacrylate) (PMMA) $M_W = 270.8$ kDa, $M_W/M_N = 1.85$, polystyrene (PS) $M_W = 212$ kDa, $M_W/M_N = 1.05$, and poly(2-vinyl pyridine) (P2VP) $M_W = 50.6$ kDa, $M_W/M_N = 1.07$ are obtained from Polymer Source, Inc. Reagent grade toluene, ethanol, isopropanol, cyclohexane, 1,2-dichloroethane, and chlorobenzene are used as received. Deionized water (18.2 M Ω cm resistivity) is produced by using a Thermo Scientific Barnstead EASYpure II UV water purifier. Prime grade low-doped $\varnothing 2''$ Si wafers (>1 Ω cm resistivity, $\langle 100 \rangle$ orientation, 0.26-0.31 mm thick, Montco Silicon Technologies, Inc.) are used as substrates. The coatings are spin-cast from polymer solutions (PS and PMMA in toluene, P2VP in isopropanol) at 3000 rpm for 60 s. The substrates are cleaned immediately before coating in oxygen plasma for 600 s. A PE-200 Oxygen Plasma Surface Treatment and Etching System at 250 W RF power and 50 cm³/min oxygen flow was used.

A. Sorption/desorption at a constant temperature

This test involves running a solvent vapor pressure program in combination with simultaneous recording of ellipsometric data for a thin polymer film on a Si substrate immersed in the vapor atmosphere at a constant temperature. Typically, ellipsometric angle Δ at the wavelength of 504 nm is monitored.¹⁵ The raw data $\Delta(t)$ and $P(t)$ can be combined into $\Delta(P)$ or $\Delta(a)$ function, where a is a degree of vapor saturation P/P_{SAT} frequently referred to as solvent activity.³⁴ Here P_{SAT} is given for the sample temperature T .

Further data processing typically involves transformation of $\Delta(a)$ to isotherms $h(a)$ or $\varphi_S(a)$ using optical modeling, where h is film thickness, and φ_S is solvent volume fraction.¹⁴ Film Wizard software version 8.0.3 by SCI is used for the modeling. The solvent-polymer combinations used in this work can be described by either of two simple film stacks. The structure “ h nm thick liquid solvent layer on a polymer layer on a substrate” is illustrated in Fig. 3(a). It is applicable to a poor solvent which does not swell the polymer and forms liquid-like ad-layer on the polymer’s free surface. The other film stack “swelled polymer layer containing φ_S volume fraction of solvent on a substrate” fits well the combinations where solvent easily penetrates into the polymer layer. It is shown in Fig. 3(b). The indices of refraction n and coefficients of extinction k for all stack materials at a given wavelength are required for the modeling. Parameters n and k for individual materials can be found in the literature or measured in a

separate experiment. All polymers and solvents used in this work are colorless; their $k = 0$ for visible light. Estimation of n for swelled polymer can be performed using Effective Media Approximation (EMA) theory.⁸ Examples of EMA calculations are given in the [supplementary material](#). It is worth to note that the composition of polymer-solvent mixture in the EMA theory is naturally expressed as the volume fractions of the components. It is assumed that the expansion or contraction of thin supported films occurs only in the direction normal to the substrate.³⁵

Conversion of the large $\Delta(a)$ data arrays to $h(a)$ or $\varphi_S(a)$ by commercially available optical modeling programs can be burdensome. While the direct problem of computing Δ for a given film stack can be accurately solved by a standard algorithm,¹⁴ the inverse problem of converting measured Δ to the layer properties requires a computationally intensive film stack optimization procedure that may generate erroneous result. Advanced modeling programs offer automation tools to organize the conversion and perform external calculations (EMA) if needed. For example, the macro language included with Film Wizard ver. 8.0.3 has a built-in function for calculation of the ellipsometric angles out of the arbitrary film stack; however, the optimization algorithm should be written by user. Since the only one independent film stack parameter is to be computed, and $\Delta(h)$ and $\Delta(\varphi_S)$ are typically smooth functions for the practical applications, less universal but much simpler interpolation approach is used in this work. Angle Δ is calculated for a small set of experimentally reasonable h or φ_S , and then tabulated $h(\Delta)$ or $\varphi_S(\Delta)$ functions are interpolated using a linear or polynomial equation.

Figure 4 demonstrates the effect of poor solvents on the 32-33 nm PS coating on a Si wafer. Nitrogen gas [Fig. 4(a)] is chosen as a medium with negligible sorption on PS. Changing pressure in the measurement chamber can cause spurious effects in the *in situ* ellipsometry by influencing mechanical stress and birefringence in quartz windows.³⁶ No noticeable $\Delta(P)$ dependence up to 95 Torr (which exceeds the vapor pressure in all other experiments) ensures that changes of Δ in the systems discussed below are caused entirely by the changes of the sample. Sorption-desorption cycles for water and isopropanol vapors are illustrated in Figs. 4(b) and 4(c), respectively. Both $\Delta(a)$ functions and $h(a)$ isotherms are given. Optical modeling for these cases assumes the formation of liquid-like water or isopropanol layer on the free surface of the PS coating. Thickness of 1 ML (monolayer) of solvent can be estimated using formula $1 \text{ ML} = \sqrt[3]{M/\rho N_A}$, where M is the molar mass, ρ is the mass density, and N_A is Avogadro’s number. For water, 1 ML = 0.31 nm; for isopropanol, 1 ML = 0.50 nm. The hydrophobic nature of the PS surface prevents the formation of the monolayer of water even at relatively high $a = 0.76$ saturation. Isopropanol demonstrates stronger interaction with the PS surface. The kink on the sorption isotherm at $a \approx 0.6$ apparently corresponds to the onset of the multilayer formation. These results illustrate setup’s capability to test adsorption on flat surfaces. A variety of possible substrates is a significant advantage of this method over the quartz microbalance technique.³⁷ The latter method is also suffering from large errors due to significant mechanical stress in the coatings.³⁸

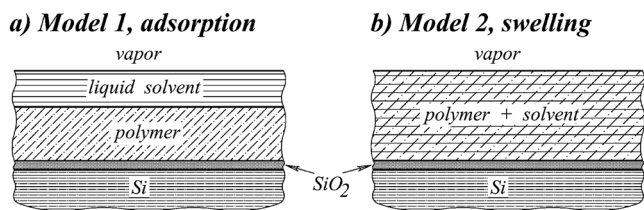


FIG. 3. Two optical models for polymer-solvent interaction used in this work.

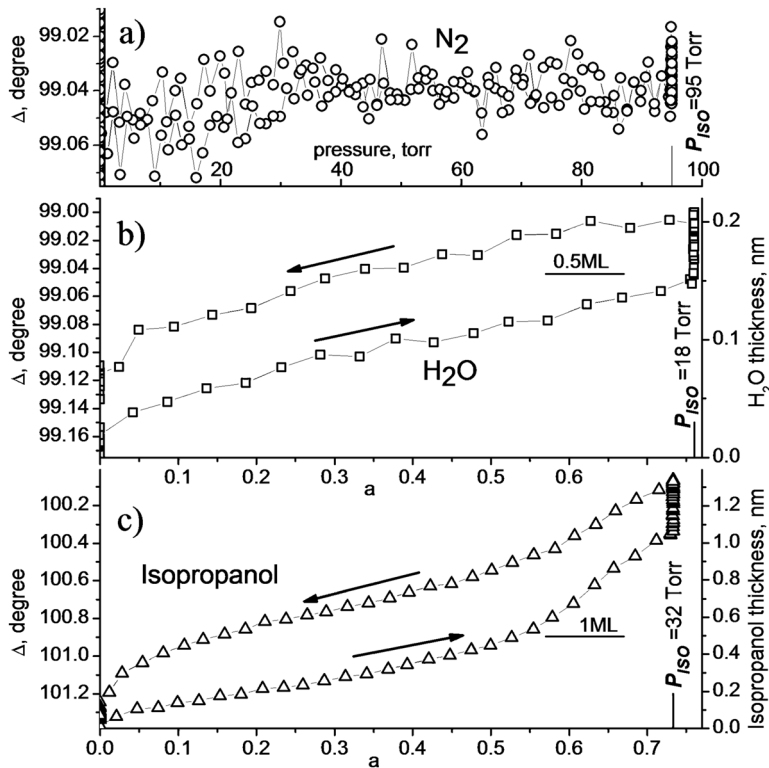


FIG. 4. Sorption and desorption of (b) water and (c) isopropanol vapor on 32-33 nm thick PS films. Dependence of Δ on pressure for non-absorbing gas, nitrogen, is shown in plot (a) for comparison. The pressure program: $v_{UP} = 4$ Torr/min, $t_{ISO} = 10$ min, and $v_{DOWN} = -4$ Torr/min. P_{ISO} for each test is denoted on the plots.

An example of polymer swelling in a vapor of a good solvent is given in Fig. 5. Optical model 2 [swelling, Fig. 3(b)], EMA for calculation of swelled polymer n , and quadratic interpolation of $\varphi_S(\Delta)$ are used. Large hysteresis between absorption and desorption curves starting at 0 pressure and ending at a_g is characteristic of this interaction. A similar hysteresis is seen in the systems PS-toluene, PS-1,2-dichloroethane, PS-chlorobenzene, and PMMA-1,2-dichloroethane. The rubbery film at high a can be well described by the Flory-Huggins equation $a = \varphi_S \exp((1 - \varphi_S) + \chi(1 - \varphi_S)^2)$, where χ is the Flory-Huggins interaction parameter.³⁹ The glass transition between the solid and rubbery regimes can be characterized by the transition saturation degree a_g where desorption curve starts to deviate from the Flory-Huggins model, by the corresponding glass transition pressure $P_g = a_g * P_{SAT}$, and by the softening point a_s , where the swelling and drying $\varphi_S(a)$ intersect.⁴⁰ An intriguing feature of accelerated desorption in

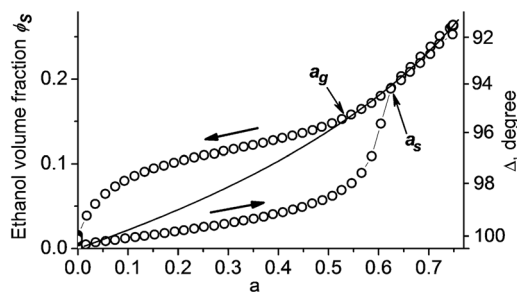


FIG. 5. Swelling and drying of P2VP in ethanol vapor (circles). Flory-Huggins model is shown by the solid line, fitted $\chi = 0.57$. Glass transition and softening points are denoted as a_g and a_s , respectively. The pressure program: $v_{UP} = 4$ Torr/min, $P_{ISO} = 44$ Torr, $t_{ISO} = 10$ min, and $v_{DOWN} = -4$ Torr/min.

the vicinity of $a = 0$ is seen in this work for all polymer-solvent combinations with the large hysteresis. A short review of possible models can be found elsewhere.⁴⁰

Figure 6 demonstrates the 3 sequential cycles of absorption and desorption of toluene vapor by 6 nm thick PS coating. It is a good illustration of the sensitivity and reproducibility of the system for probing polymer-solvent interaction in extremely thin films. For example, $a_g = 0.517 \pm 0.003$, where the error is the standard deviation of the a_g data calculated for individual cycles.

B. Temperature programmed desorption (TPD)

These tests are performed as follows. After vapor exposure, thin film sample is pumped down by all 3 pumps and is subjected to a temperature cycling at a certain ramp rate.

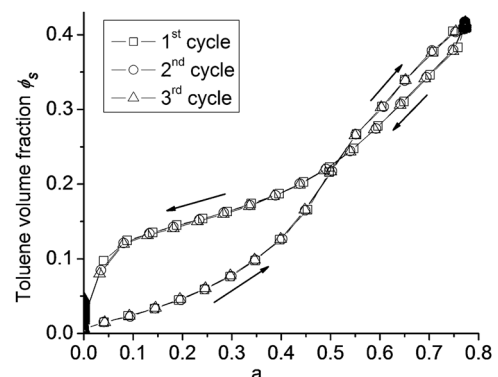


FIG. 6. Three consecutive cycles of swelling and drying of 6 nm thick PS film in toluene vapor. The pressure program: $v_{UP} = 4$ Torr/min, $P_{ISO} = 22$ Torr, $t_{ISO} = 10$ min, and $v_{DOWN} = -4$ Torr/min.

Maximal temperature T_{MAX} is chosen to be well above the glass transition temperature T_g but within the range where no decomposition occurs. $T_{MAX} = 180^\circ\text{C}$ for PMMA and 160°C for PS and P2VP coatings. Typically the first temperature cycle is immediately followed by 2 additional control cycles. As with the sorption/desorption tests, the angle Δ at the wavelength of 504 nm is monitored. The raw data $\Delta(t)$ and $T(t)$ are combined to calculate $\Delta(T)$; following numerical differentiation yields $d\Delta/dT(T)$ function. The TPD data can be represented as the $d\Delta/dT(T)$ function difference between the first heating and the average of all subsequent heatings. The subtraction of the average removes the background thermal expansion from the TPD data. In a typical case, there is no significant difference between the cooling and heating (excluding the 1st) curves, so the average can include both curve types. Representation of the TPD in the form of $d\varphi_S/dT(T)$ or $dh/dT(T)$ data can be more desirable due to its clearer physical meaning. However, $d\Delta/dT(T)$ to $d\varphi_S/dT(T)$ conversion depends on the optical model. Similar to the sorption-desorption data treatment, the interpolation method can be used for the conversion. Typically the change of Δ during TPD is small enough to use linear interpolation.

The choice of optical model requires a special consideration. A polymer film after solvent annealing and drying may contain residual solvent,^{41,42} voids,⁴³ or both of them. Model 2 [Fig. 3(b)] can be used in all these cases; the only difference is the refractive index n of the composite computed by EMA. In this work, the TPD data are represented as $d\Delta/dT(T)$ with additional right-side axes representing two limiting models: solvent model is the Model 2 containing polymer-solvent composite, voids model contains polymer-voids composite. For simplicity, changes of optical constants with temperature are considered as a negligible factor.

The TPD curves for PMMA [Fig. 7(a)] and P2VP [Fig. 7(b)] coatings after exposure to vapors of good solvents above P_g display 2 peaks associated with the film contraction; the background of the natural thermal expansion is removed from the TPD data and is shown by open symbols.

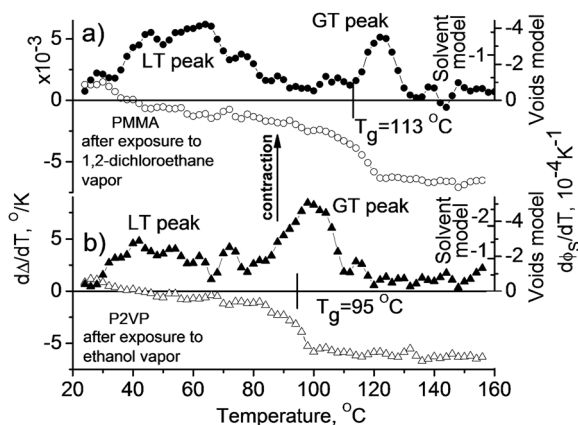


FIG. 7. TPD curves for 30 nm thick PMMA film after exposure to 1,2-dichloroethane vapor (solid circles) and for 32 nm thick P2VP film after exposure to ethanol vapor (solid triangles). Open symbols show behavior of the thermally annealed films. The vapor exposure pressure program for both samples: $v_{UP} = 4$ Torr/min, $t_{ISO} = 10$ min, and $v_{DOWN} = -4$ Torr/min. P_{ISO} for 1,2-dichloroethane is 56 Torr; for ethanol is 44 Torr.

The relatively narrow GT (glass transition) peak appears in the vicinity of the glass transition where the jump in molecular mobility speeds up the departure of solvent or voids from the film. The broad LT (low temperature) peak has the onset close to the starting TPD temperature and spans typically up to 60–80 °C. This peak also depends on the previous exposure to the solvent vapor. The features on the TPD curves for all systems investigated in this work can be classified as either GT or LT peak. The TPD spectra of the investigated systems will be discussed in detail in a separate publication.

The set of TPD curves for 6 nm PS coating presented in Fig. 8 is a good illustration of sensitivity and reproducibility of the TPD analysis in the discussed setup.

C. Additional considerations

The ability to perform thermal annealing on the samples is very advantageous for the reproducibility and throughput of the solvent annealing studies. Multiple use of the same sample in a variety of experiments requires restoring the sample to the initial, standard, or well characterized state at the beginning of each test. For good solvents, the solvent annealing above the glass transition (at $a > a_S$) is often used to erase the sample's history.⁴⁰ However, for many systems, a_S can be hard to reach or non-existent. For some systems, keeping them in a rubbery state for a reasonable time does not erase the material's memory completely.^{40,44} Thermal annealing at the temperatures above T_g for glass-forming coatings offers a more universal method of sample rejuvenation. Thermal annealing of coatings at 160 °C (PS, P2VP) or 180 °C (PMMA) for 1 h precedes all solvent annealing experiments presented in this work. It is noteworthy that the state of the sample after the thermal annealing above T_g differs from the state yielded by the solvent annealing in a rubbery state. A simple experiment demonstrating this difference consists of 2 cycles of solvent annealing above a_S after an initial thermal annealing above the T_g . Then, the second cycle has the solvent annealed sample as the initial state. As demonstrated in Fig. 9, the PS film after thermal annealing at 160 °C is characterized

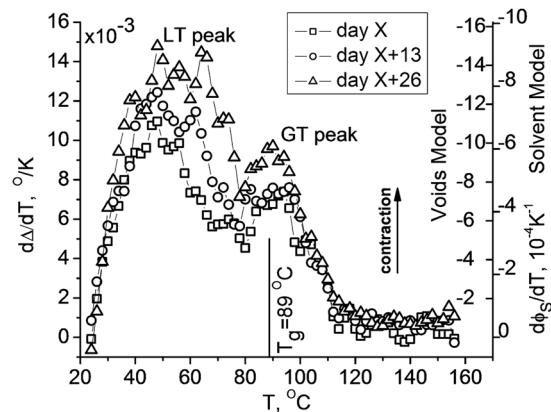


FIG. 8. TPD curves for the same 6 nm thick PS film after exposures to toluene vapor. Extensive testing of the PS sample between the shown TPD experiments includes about 10 solvent annealings and 30 thermal cycles between the day X and the day X + 13; 10 thermal cycles between the day X + 13 and the day X + 26. The vapor exposure pressure program for all TPD consists of: $v_{UP} = 4$ Torr/min, $P_{ISO} = 22$ Torr, $t_{ISO} = 10$ min, and $v_{DOWN} = -4$ Torr/min.

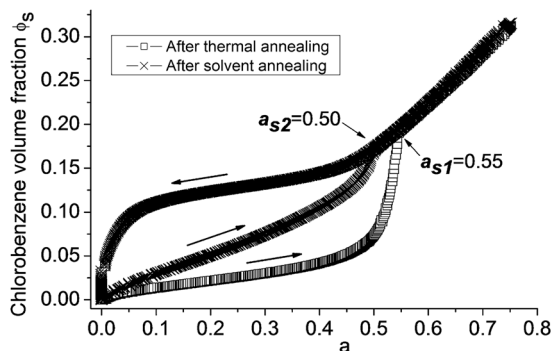


FIG. 9. Two consecutive cycles of swelling and drying of 170 nm thick PS film in chlorobenzene vapor. The pressure program: $v_{UP} = 0.05$ Torr/min, $P_{ISO} = 9$ Torr, $t_{ISO} = 10$ min, and $v_{DOWN} = -0.05$ Torr/min.

by larger hysteresis and better “resistance” to transformation to the rubbery state (larger a_S) than the solvent annealed sample.

The possibility for the polymer coatings to develop a morphology and ultimately to dewet the substrate should be taken into consideration. All coatings described here were analyzed by AFM in previous studies.^{15,45–47} No dewetting or significant surface roughening was found for both as-spun films and coatings after similar temperature treatment. As a significant advantage of the presented design, the roughening and dewetting processes are readily detectable by the ellipsometry and form a pronounced characteristic pattern on the ellipsometric angles vs time dependencies. These processes manifest themselves as an apparent increase of the film thickness.^{46,47} In all systems tested for this work, Δ angle is returning practically to the initial value after all sorption-desorption and heating-cooling cycles (with the correction to the residual solvent or voids). It represents a strong argument for the absence of any irreversible morphology or dewetting formed in these tests.

It is also worth to note that utilizing multi-wavelength ellipsometric measurements, available for the present design, can be particularly useful for probing anisotropic films and samples with complicated film stack and morphology.^{14,48} Processing of the spectroscopic data arrays may require additional programming efforts to design a multi-spectrum optimization procedure.¹⁴

IV. CONCLUSIONS

An experimental setup is designed for probing polymer film–solvent vapor interaction. The instrument is made of an environmental chamber combined with an *in situ* spectroscopic ellipsometer, controlled temperature sample stage, and vapor pressure control system and employs oil-free vacuum pumps. Solvent vapor sorption-desorption isotherms and temperature programmed desorption (TPD) spectra are available as dependencies of ellipsometric angles or film thickness on either vapor pressure or sample temperature. Both isotherms and TPD data can be obtained from the same sample without removing it from the chamber. Sophisticated measurement and sample treatment sequences are made effortless by the extensive automatization. Computer control eliminates operator’s

involvement in the experimental run which is advantageous for reproducible results. The performance of the vapor pressure control system is characterized by using vapors of toluene, 1,2-dichloroethane, cyclohexane, isopropanol, water, ethanol, and chlorobenzene. Possible applications are demonstrated using 6–170 nm thick glass-forming polymer (PS, P2VP, and PMMA) coatings on silicon wafers. The applications include recording TPD curves for polymer films after solvent vapor exposure, adsorption-desorption isotherms for weak-interacting polymer-vapor pairs, and absorption-desorption isotherms for polymers immersed in a vapor of a good solvent. Applicability of the instrument for testing a few nanometers thick coatings is shown. Practical methods of the ellipsometric data analysis are discussed.

SUPPLEMENTARY MATERIAL

See [supplementary material](#) for the detailed characteristics of the solvent vapor pressure control system test runs and for the examples of the EMA calculations.

ACKNOWLEDGMENTS

This research is partially supported by the University of Wisconsin-Madison College of Engineering Shared Research Facilities and the NSF through the Materials Science Research and Engineering Center (No. DMR-1720415) using instrumentation provided at the UW-Madison Materials Science Center.

- ¹Directed Self-Assembly of Block Copolymers for Nano-Manufacturing, 1st ed., edited by R. Gronheid and P. Nealey (Elsevier, 2015).
- ²R. A. Lawson and A. P. G. Robinson, “Overview of materials and processes for lithography,” in *Frontiers of Nanoscience*, 1st ed., edited by A. P. G. Robinson and R. A. Lawson (Elsevier, 2016), Vol. 11, pp. 1–90.
- ³S. Ji, L. Wan, C. Liu, and P. F. Nealey, *Prog. Polym. Sci.* **54–55**, 76 (2016).
- ⁴M. A. Morris, *Microelectron. Eng.* **132**, 207 (2015).
- ⁵S.-J. Jeong, J. Y. Kim, B. H. Kim, H.-S. Moon, and S. O. Kim, *Mater. Today* **16**, 468 (2013).
- ⁶C. Jin, B. C. Olsen, E. J. Lubner, and J. M. Buriak, *Chem. Mater.* **29**, 176 (2017).
- ⁷N. L. Thomas and A. H. Windle, *Polymer* **23**, 529 (1982).
- ⁸K. Manoli, D. Goustouridis, S. Chatzandroulis, I. Raptis, E. S. Valamontes, and M. Sanopoulou, *Polymer* **47**, 6117 (2006).
- ⁹U. Zettl, A. Knoll, and L. Tsarkova, *Langmuir* **26**, 6610 (2010).
- ¹⁰G. C. Abuin, M. C. Fuertes, and H. R. Corti, *J. Membr. Sci.* **428**, 507 (2013).
- ¹¹Y. Li, E. J. Park, K. T. Lim, K. P. Johnston, and P. F. Green, *J. Polym. Sci., Part B: Polym. Phys.* **45**, 1313 (2007).
- ¹²A. Serghèi, H. Huth, M. Schellenberger, C. Schick, and F. Kremer, *Phys. Rev. E* **71**, 061801 (2005).
- ¹³A. Serghèi and F. Kremer, *Macromol. Chem. Phys.* **209**, 810 (2008).
- ¹⁴H. Fujiwara, *Spectroscopic Ellipsometry: Principles and Applications* (John Wiley & Sons, Ltd., The Atrium, Southern Gate, Chichester, West Sussex PO19 8SQ, England, 2007).
- ¹⁵M. Yu. Efremov, S. S. Soofi, A. V. Kiyanova, C. J. Munoz, P. Burgardt, F. Cerrina, and P. Nealey, *Rev. Sci. Instrum.* **79**, 043903 (2008).
- ¹⁶W. Ogieglo, H. Wormeester, K.-J. Eichhorn, M. Wessling, and N. E. Benes, *Prog. Polym. Sci.* **42**, 42 (2015).
- ¹⁷R. J. Archer, in *Ellipsometry in the Measurement of Surfaces and Thin Films, Symposium Proceedings, Washington 1963*, edited by E. Passaglia, R. R. Stromberg, and J. Kruger (National Bureau of Standards, Washington, DC, 1964), pp. 255–280.
- ¹⁸M. L. Gee, T. W. Healy, and L. R. White, *J. Colloid Interface Sci.* **131**, 18 (1989).

- ¹⁹M. R. Baklanov, K. P. Mogilnikov, V. G. Polovinkin, and F. N. Dultsev, *J. Vac. Sci. Technol., B: Microelectron. Nanometer Struct.–Process., Meas., Phenom.* **18**(3), 1385 (2000).
- ²⁰A. Bourgeois, Y. Turcant, Ch. Walsh, and Ch. Defranoux, *Appl. Surf. Sci.* **256S**, S26 (2009).
- ²¹Y. Zheng and G. B. McKenna, *Macromolecules* **36**, 2387 (2003).
- ²²M. Alcoutlabi, L. Banda, K. Kollengodu-Subramanian, J. Zhao, and G. B. McKenna, *Macromolecules* **44**, 3828 (2011).
- ²³Y. Zheng, R. D. Priestley, and G. B. McKenna, *J. Polym. Sci., Part B: Polym. Phys.* **42**, 2107 (2004).
- ²⁴Z. Fakhraai and J. A. Forrest, *Science* **319**, 600 (2008).
- ²⁵P. L. Skousen, *Valve Handbook* (The McGraw-Hill Co., Inc., New York, NY, 1998).
- ²⁶*Perry's Chemical Engineers' Handbook*, 7th ed., edited by R. H. Perry, D. W. Green, and J. O. Maloney (The McGraw-Hill Co., Inc. New York, NY, 1997).
- ²⁷C. L. Smith, *Practical Process Control: Tuning and Troubleshooting* (John Wiley & Sons, Inc., Hoboken, NJ, 2009).
- ²⁸K. Ogata, *Modern Control Engineering*, 4th ed. (Prentice Hall, Inc., Upper Saddle River, NJ, 2002).
- ²⁹ASTM Standard D1418-17 Standard Practice for Rubber and Rubber Latexes—Nomenclature, ASTM International, 100 Barr Harbor Dr., P.O. Box C700, West Conshohocken, PA 19428-2959, 2017.
- ³⁰*Parker O-Ring Handbook* (Parker Hannifin Corp., Cleveland, OH, 2007).
- ³¹DuPont Kalrez, Technical Information, Rev. 11, 2012.
- ³²Chemraz Product Data, Greene, Tweed, 1930 Rankin Road, Houston, TX, 2016.
- ³³Parker O-Ring Material Offering Guide, Parker Hannifin Corp., Cleveland, OH, 2014.
- ³⁴C. Wohlfarth, “Vapor pressures (solvent activities) for binary polymer solutions,” in *CRC Handbook of Chemistry and Physics*, 98th ed., edited by J. R. Rumble (CRC Press/Taylor & Francis, Boca Raton, FL, 2018), pp. 13–40.
- ³⁵B. W. Rowe, B. D. Freeman, and D. R. Paul, *Macromolecules* **40**, 2806 (2007).
- ³⁶K. A. Conrad, R. K. Sampson, H. Z. Massoud, and E. A. Irene, *Rev. Sci. Instrum.* **67**, 3954 (1996).
- ³⁷V. Tsionsky and E. Gileadi, *Langmuir* **10**, 2830 (1994).
- ³⁸L. Banda, M. Alcoutlabi, and G. B. McKenna, *J. Polym. Sci., Part B: Polym. Phys.* **44**, 801 (2006).
- ³⁹P. J. Flory, *Principles of Polymer Chemistry* (Cornell University Press, Ithaca, NY, 1953).
- ⁴⁰F. Doumenc, H. Bodiguel, and B. Guerrier, *Eur. Phys. J. E* **27**, 3 (2008).
- ⁴¹X. Zhang, K. G. Yager, S. Kang, N. J. Fredin, B. Akgun, S. Satija, J. F. Douglas, A. Karim, and R. L. Jones, *Macromolecules* **43**, 1117 (2010).
- ⁴²J. Perlich, V. Körstgens, E. Metwalli, L. Schulz, R. Georgii, and P. Müller-Buschbaum, *Macromolecules* **42**, 337 (2009).
- ⁴³I. Lopez Garcia, J. L. Keddie, and M. Sferrazza, *Surf. Interface Anal.* **43**, 1448 (2011).
- ⁴⁴A. Laschitsch, C. Bouchard, J. Habicht, M. Schimmel, J. Rühe, and D. Johannsmann, *Macromolecules* **32**, 1244 (1999).
- ⁴⁵M. Yu. Efremov, A. V. Kiyanova, J. Last, S. S. Soofi, C. Thode, and P. Nealey, *Phys. Rev. E* **86**, 021501 (2012).
- ⁴⁶M. Yu. Efremov, C. Thode, and P. Nealey, *Rev. Sci. Instrum.* **84**, 023905 (2013).
- ⁴⁷M. Yu. Efremov, *Rev. Sci. Instrum.* **85**, 123901 (2014).
- ⁴⁸B. B. Sauer and D. J. Walsh, *Macromolecules* **27**, 432 (1994).